

IMAGING OPTICAL INTERFEROMETRY

R. S. SIMON¹, K. J. JOHNSTON², D. MOZURKEWICH², K. W. WEILER²,
 D. J. HUTTER³, J. T. ARMSTRONG⁴, and T. S. BRACKETT¹

¹Interferometrics Inc., 8150 Leesburg Pike, Vienna, VA 22182-2799

²Center for Advanced Space Sensing, Code 4200, Naval Research Laboratory,
 Washington, D.C. 20375-5000

³Astrometry Division, US Naval Observatory, 34th & Massachusetts Ave., N.W.,
 Washington, D.C. 20392-5100

⁴Universities Space Research Association, 600 Maryland Ave., S.W., Suite 303,
 Washington D.C. 20024

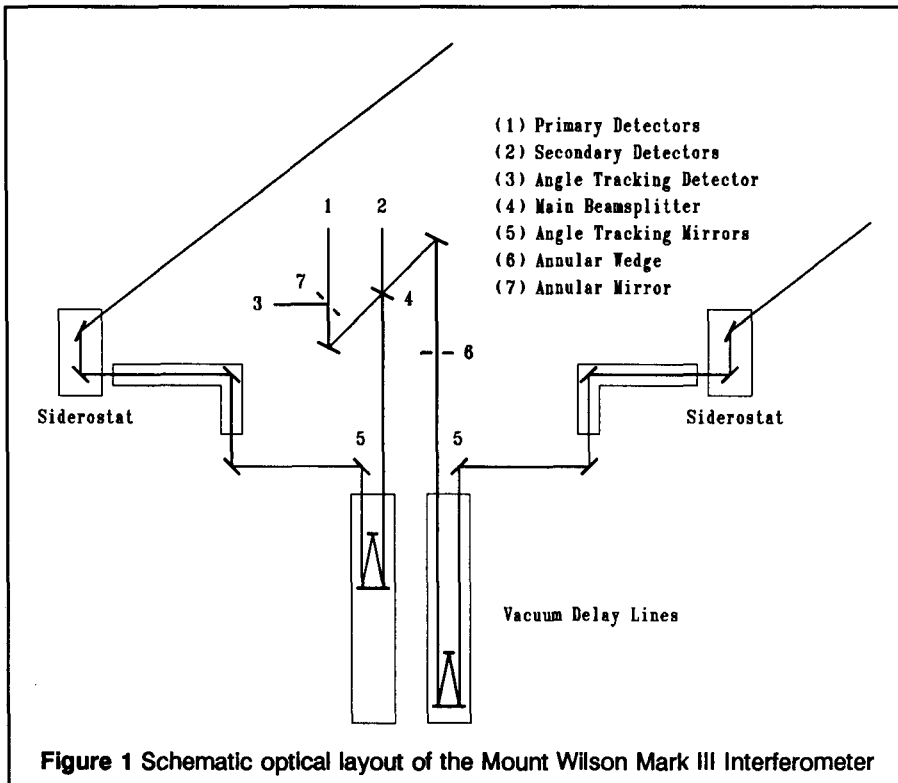
ABSTRACT Interferometry at optical wavelengths is very similar to radio interferometry, once the fundamental differences in detectors are accounted for. The Mount Wilson Mark III optical interferometer has been used for optical interferometry of stars and stellar systems. Success with the Mark III has led to the current program at the Naval Research Laboratory to build the Big Optical Array (BOA), which will be an imaging interferometer. Imaging simulations show that BOA will be able to produce images of complex stellar systems, with a resolution as fine as 0.2 milliarcseconds.

INTRODUCTION

Optical interferometry techniques have advanced to the point where it is possible to build arrays at optical wavelengths which can do many of the types of observations routinely done with interferometric arrays at radio wavelengths. This paper will introduce optical interferometry techniques with an emphasis on the differences between radio and optical interferometry, discuss an example of an optical interferometer (the Mount Wilson Mark III interferometer), summarize the NRL/USNO Optical Interferometer Project which is building both the Big Optical Array (BOA) and the USNO Astrometric Interferometer, and then discuss BOA and its imaging potential in more detail.

A Simple Interferometer

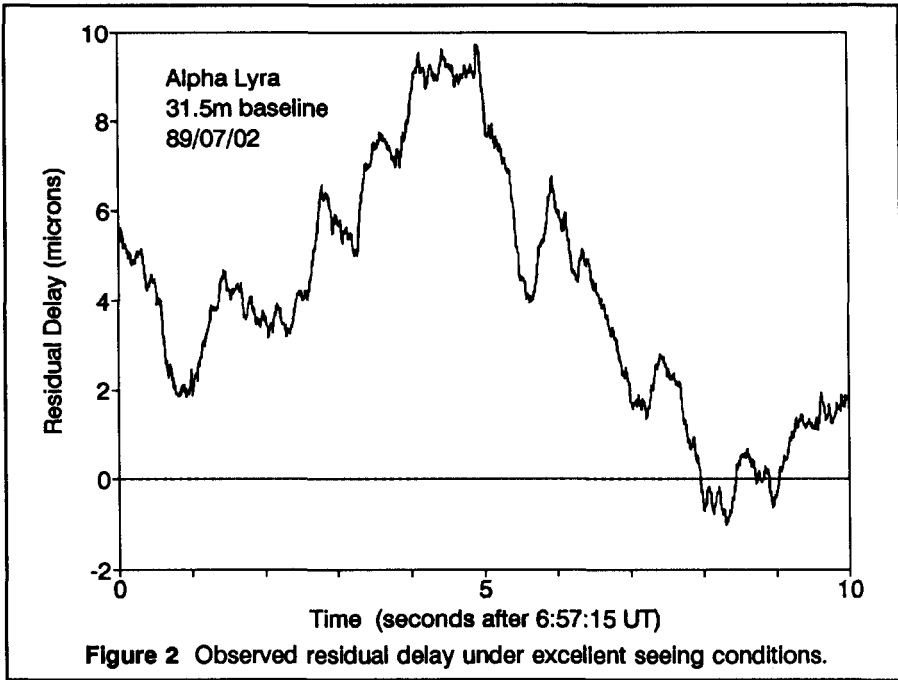
Figure 1 shows a schematic diagram of a simple optical interferometer, based on the Mount Wilson Mark III Optical Interferometer (Shao *et al.* 1988). This instrument was developed under a joint Office of Naval Research program by NRL, the Smithsonian Astrophysical Observatory, the US Naval Observatory, and the Massachusetts Institute of Technology. At the left and right in Figure 1, siderostats and fixed mirrors direct starlight to the center of the interferometer. Angle tracking mirrors driven actively by PZTs



reflect the beams into the delay lines and provide small angle pointing corrections. The retroreflectors in the vacuum delay lines move to precisely compensate for the different path lengths on each side of the interferometer. One delay line length is modulated to sample a $\lambda/2$ range of delay and make the fringes detectable, while the other is changed continuously to compensate for the sidereal motion of the star. The beam on the right in Figure 1 goes through an annular wedge which introduces an angular offset in the outer annulus of the beam for tracking purposes. The light beams are finally combined at the main beam splitter, with the output beams directed by fixed mirrors to photon detectors; one beam passes through an annular mirror used to direct the outer annulus of the beam to the star tracker camera.

INTERFEROMETRY AT RADIO AND OPTICAL WAVELENGTHS

There are several fundamental differences between doing interferometry at radio wavelengths and doing it at optical wavelengths. The most fundamental difference is that there are no broadband coherent amplifiers (detectors) at optical wavelengths. For observations using visible wavelengths, the band of 450 to 900 nm corresponds to a central frequency of 667 THz, and a bandwidth of 333 THz. Besides the present limits of detector technology when considering such bandwidths, quantum mechanical limits will never allow coherent detectors to operate with such a large bandwidth at low photon rates; narrower bandwidths are too insensitive for astronomical sources.



The lack of coherent detectors at optical wavelengths has several important implications: (1) Optical interferometry is additive interferometry, rather than the multiplicative interferometry normally used at radio wavelengths. (2) Detection of the signal must occur after the light has been combined. This means that simultaneous detection on many baselines requires that the incident starlight be split up, and results in a reduced signal to noise ratio. (3) Path length delays must be introduced physically at optical wavelengths rather than electrically at some convenient IF frequency.

The difficulties of working at optical wavelengths are compensated by the availability of very broad band detectors, so that good sensitivity can still be achieved.

For ground based optical interferometry, the atmosphere defines fundamental sensitivity limits. Turbulence in the atmosphere limits the coherence length r_0 (the Fried parameter; see Fried 1965) for a wavefront, causing poor astronomical seeing. The typical value of r_0 at visible wavelengths is about 10 cm, with values ranging from ~ 5 cm or less under poor conditions to 30-40 cm under superb conditions at the best sites. For active fringe detection and tracking, the useful siderostat aperture is limited to $\sim r_0$ or less to prevent reductions in fringe visibility. Since the lowest order effect of turbulence is to cause image wander, active pointing corrections which remove the effects of wavefront tilts are useful and increase the effective r_0 by ~ 3.4 times (Fried 1965).

A further limitation is that the atmospheric coherence time τ_0 is typically 10 ms. The result is that fringe detection and measurement requires detecting enough photons in a single short integration time to determine the fringe visibility and phase using a small aperture (10-40 cm). Otherwise, the fringe visibility will be reduced too much to be detectable. This requirement imposes a **fundamental** limit to the sensitivity of a phase tracking interferometer of around 10-12th magnitude in the visual. The small value of τ_0 imposes practical difficulties as well; high speed mechanical servo loops are required to correct the delay and pointing errors caused by the atmosphere. In Figure 2, a few

seconds of data taken with the Mark III interferometer are shown to demonstrate the rapid delay fluctuations caused by the atmosphere (geometric effects have been removed from the data; the data were taken under superb seeing, with $r_0 \approx 30\text{--}40$ cm). Incoherent, multi- r_0 integration techniques may avoid this sensitivity limit for ground based systems (for example, see Hughes and Hutter 1990), but the integration times become extremely long and may not be practical for an imaging system. Space based systems avoid the atmospheric r_0 limits, but may still experience, in effect, a short r_0 caused by spacecraft vibration.

Other practical difficulties faced by optical interferometers arise from dispersion in air. Unequal path lengths through air for the light from different interferometer elements results in a smearing of the broadband fringe visibility which must be corrected or avoided to preserve fringe visibility. That is, there must be equal dispersion for the different light paths in an interferometer. As is normal for interferometers in the plane-parallel atmosphere limit, the geometric delay in an optical interferometer occurs in vacuum (above the atmosphere) so that the pathlengths through the atmosphere from the star to the array elements are essentially equal. Therefore, if equal dispersion for each element in an optical interferometer is to be maintained the delay lines must be in vacuum to allow the widest possible bandwidth to be used. Alternative approaches which use either extremely narrow bandwidths and no dispersion compensation or moderate bandwidths and dispersion compensating glass (e.g., see Lacasse and Traub, 1988) reduce overall system sensitivity by the reduction in bandwidth.

A further complication is that atmospheric turbulence causes fluctuations in the differential dispersion and delay between two elements which must be actively compensated for if fringe tracking is to work (Colavita 1990). The variance of the fringe motion in delay σ^2 in radians² (Fried 1965, Colavita 1990) is $\sigma^2 = 6.9(B/r_0)^{5/3}$ where B is the baseline length. As pointed out by Colavita, this effect can result in large excursions of the nominal delay for the interferometer. For example, the nominal delay on a 500 m baseline could fluctuate ~ 300 microns rms in 1 arcsecond seeing on timescales of ~ 4 minutes. Active compensation for this effect requires accurate knowledge of the baseline geometry.

THE MOUNT WILSON MARK III OPTICAL INTERFEROMETER

The Mark III Interferometer is the only phase tracking optical interferometer currently in operation. It can observe one baseline at a time, from a selection of baselines ranging from 3 m to 31.5 m in length. Evacuated delay lines with an automated, high speed servo system allow the detection and tracking of white light fringes in real time. Details of the original configuration of the Mark III interferometer have been presented by Shao *et al.* (1988). During 1988, a variable length, north-south baseline was added to the interferometer which greatly increased its capability for measuring stellar diameters and binary systems.

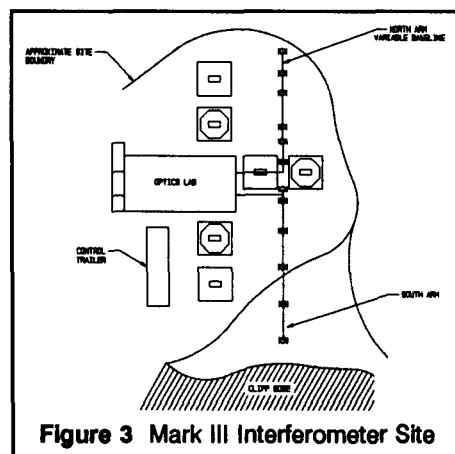


Figure 3 Mark III Interferometer Site

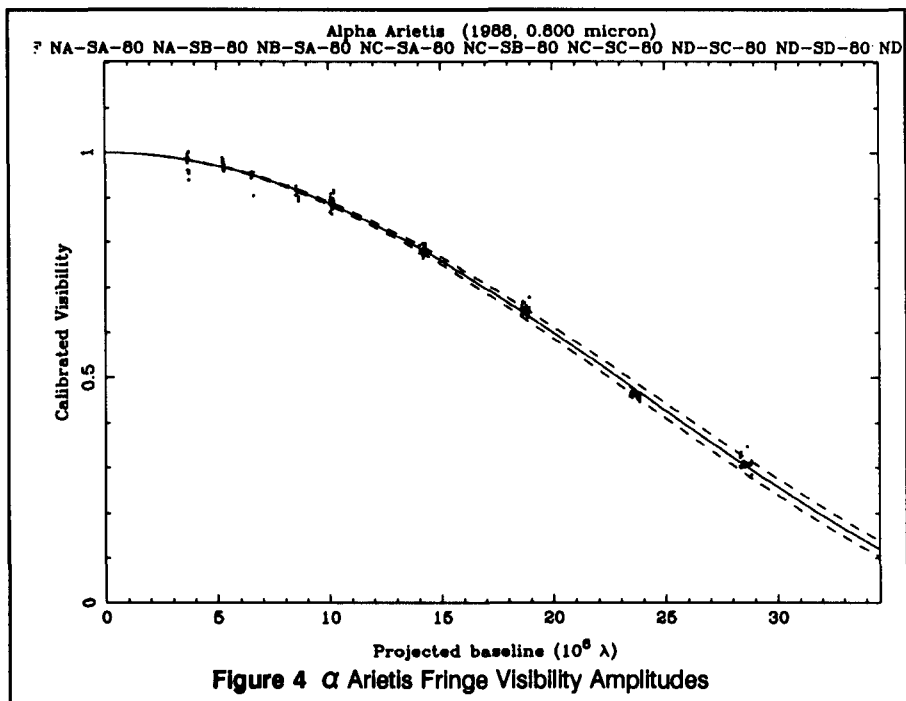
Figure 1 (above) shows the optical layout used by the Mark III; Figure 3 shows the current site configuration for the Mark III Interferometer.

Accurate diameters of stars may be measured by combining visibility measurements from several different baselines. For example, Figure 4 shows the observed (small dots) and model (solid line) visibilities for the star α Arietis. Projected baseline lengths vary from 3.5 to 29 million wavelengths (2.8 to 23 m at $\lambda=0.80 \mu$); the solid line shows the predicted visibility for the best-fit 6.41 milliarcsecond diameter uniform disk, and the dashed lines show the visibility for diameters $\pm 2\%$, corresponding to an estimated 2-sigma error of 0.12 milliarcseconds. Details of the diameter measurements and calibration procedures are presented in Simon *et al.* (1990) and Mozurkewich *et al.* (1991). Results with the Mark III agree well with previously measured diameters; our diameter of $5.26 \pm .05$ mas for the star α Canis Minoris is in excellent agreement with the diameter measured by Hanbury-Brown *et al.* (1974).

The Mark III interferometer has demonstrated the potential of interferometers for accurate wide angle astrometry of stars. Mozurkewich *et al.* (1988) and Shao *et al.* (1990) present the first astrometric results from the Mark III, obtaining stellar positions with formal errors of roughly 10 mas.

THE NRL/USNO OPTICAL INTERFEROMETER PROJECT

The Naval Research Laboratory and the US Naval Observatory are presently carrying out a project to build two separate optical interferometers: the Naval Research Laboratory Big Optical Array (BOA), and the USNO Astrometric Interferometer, using

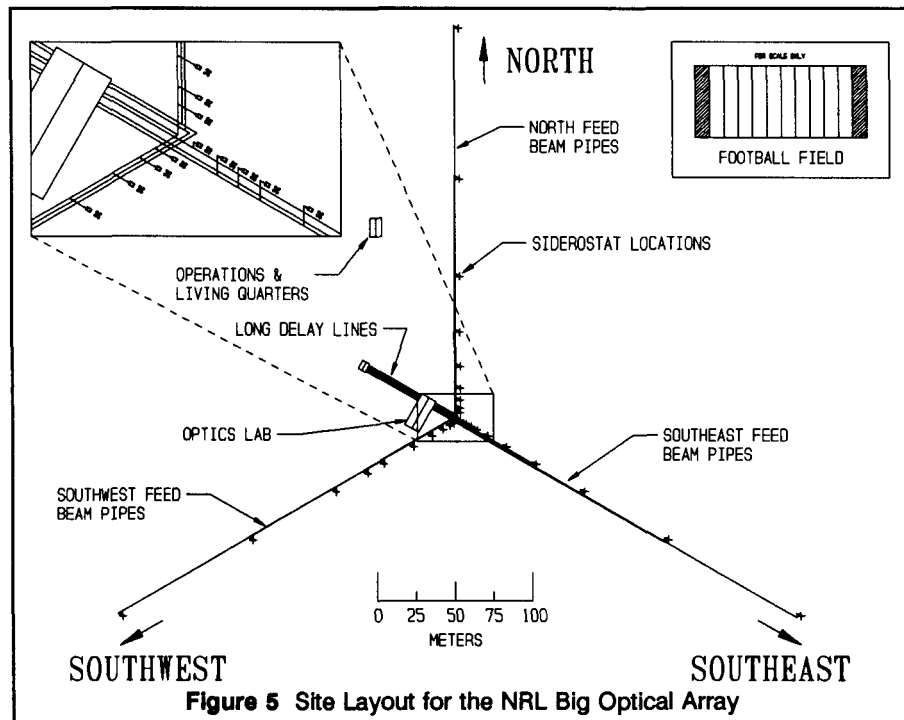


the experience gained building and operating the Mark III interferometer. The two instruments have different, complementary goals: The Astrometric Interferometer (Hughes and Hutter, 1990) will use four large (1 m) siderostats on fixed 20–40 m baselines for astrometry on stars and bright quasars. Although it will be capable of detecting fringes on quasars to $\sim m_v=15$, imaging sources that faint would be impractical due to the extremely long incoherent integration times required. The primary goal for BOA (summarized below, as well as in Mozurkewich *et al.* 1990) will be to produce images of stars and stellar systems using standard interferometric techniques, including the use of self calibration methods and phase closure to recover phase information. Here we discuss the imaging potential of optical interferometry.

THE BIG OPTICAL ARRAY

BOA will have six ~ 50 cm siderostats in a reconfigurable Y-shaped array, and will be used to form images of stars and stellar systems. The layout of BOA is shown in Figure 5. Vacuum pipes go out each arm to the siderostat stations (marked by crosses). The orientation of the array will be approximately as shown, but may be rotated by a few degrees as dictated by site topography. The inset shows a closeup of the inner part of the array. The instrumental specifications and estimated performance limits for BOA are summarized in Table I.

Phases will be simultaneously measured on multiple baselines by BOA, allowing closure phases to be used for imaging. Depending on the mode of operation, BOA will be able to make measurements ranging from simple diameter measurements of large



numbers of stars to true images of complex stellar systems.

BOA will be close to an ideal instrument interferometric imaging at optical wavelengths. It will have at least 16 wavelength channels, and in each wavelength channel up to fifteen baselines and ten closure phases can be measured simultaneously. Movable siderostats will allow the array resolution to be scaled to obtain the spatial frequencies needed for imaging the source.

Figures 6 and 7 show the (u, v) plane sampling achieved by BOA by combining observations from 3 different array configurations, for single wavelength (Figure 6) and multiple wavelength (Figure 7) observations. It is expected that the normal observing mode will use spectral channels which cover the wavelength range from $\lambda = 450$ nm to 900 nm, so that the (u, v) coverage shown in Figure 7 will often be realized. In Figure 6, only the data from a single wavelength channel in the red is included, as might be the case for narrow band observations. As Figure 7 suggests, the use of multi-frequency synthesis techniques will be extremely valuable with BOA. Such techniques both greatly increase the coverage in the (u, v) plane and also allow fringe detection at long wavelengths (where the SNR is usually higher) to help fringe detection at shorter wavelengths (where the resolution is doubled!). The improvement afforded by multi-frequency synthesis means that the multi-wavelength observing mode will be far more capable of observing complex images than the single wavelength observing mode.

In one mode of operation the array will be phased on the observed object. This will be accomplished by detecting and actively tracking the fringes over short, redundant baselines between individual mirrors. Fringe tracking in this mode is actually a form of adaptive optics, where the aperture being phased up is several hundred meters in diameter. The internal path lengths in the beam combining optics have been set up in such a way that fringes have to be detected on only five of the fifteen baselines to phase the entire array. It includes five equally short baselines in each configuration. These short baselines are used for tracking fringes. Once the array is phased, data on the long baselines can be coherently averaged until the desired signal to noise is reached. Even with a visibility amplitude of 0.01 (1 percent of the flux is unresolved) a signal to noise of 100 can be obtained on bright stars with integration times of 5 minutes or less.

This "bootstrap phasing" capability of the BOA is absolutely critical for making good images of stars unless we can phase the array using some external mechanism. If external phasing is possible, we will not need the short, redundant baselines and better

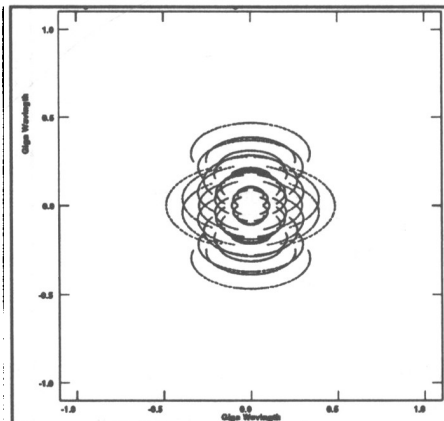


Figure 6 BOA narrow-band u, v coverage

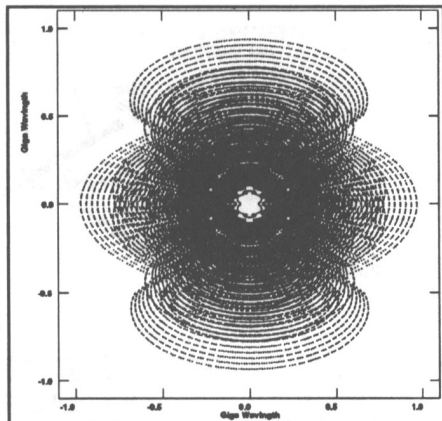


Figure 7 BOA wide-band u, v coverage

TABLE I BOA Instrumental Characteristics

Number of Array Elements:	6
Baseline Lengths:	4 meters to 470 meters
Array Configuration:	(3) 251 m arms, Y-shaped
Maximum Usable Aperture:	35 cm clear aperture from 50 cm siderostat
Long Delay Lines (6):	0-420 meter optical path length, folded in 4
Fast Delay Lines (6):	0-6 meter optical path length, folded in 2
Beam Combination Options:	2 baselines with 2-way combination, or 2 3-way combinations, with closure phase, or 1 6-way combination, all baselines at once
Dispersion Compensation:	Vacuum delay lines, compensating glass
Fringe Detection:	Multi-channel spectral fringe processor
Real Time Control System:	VX-Works, VME-bus, 680xx processors
Limiting Visual Magnitude:	~ 10 (with high visibility) ~ 9.5 (diameter measurements) ~ 4.5 (imaging mode) ~ 11-12 (ideal conditions, improved detectors)
Resolution:	
Smallest Configuration:	0.04 arcseconds (~4 m baselines, $\lambda=900$ nm)
Largest Configuration:	0.0002 arcseconds (470 m baselines, $\lambda=450$ nm)
Visibility Errors:	$\leq 1\%$
Stellar Diameter Errors:	1% accuracy
Image Dynamic Ranges:	$\geq 100:1$
Wavelength Range:	450 nm to 900 nm initially (IR enhancements feasible)

imaging can be obtained with the same number of telescopes.

IMAGING SIMULATIONS WITH THE BIG OPTICAL ARRAY

To test the imaging capability of the BOA, we have performed several computer simulations on test images. For the simulations, the following steps were used:

- (1) Create a test image.
- (2) Generate an artificial data set containing simulated interferometric measurements of the test image, with realistic noise.
- (3) Use standard image reconstruction algorithms to produce a final simulated image.

As an example, for one of the simulations a test source resembling a very active star was used. The array configuration selected was scaled to be ideal for a third magnitude star of spectral type F III. Such a star should have a diameter of about 1.6 mas and provide about 250 photons per 4 ms integration time. This simulation used 16 wavelength channels of BOA spanning 450 to 900 nm in even wavelength steps. The simulated data used three different configurations of BOA, with 6 siderostats used in each configuration. The (u, v) plane coverage is shown in Figure 7.

We assumed systematic calibration errors of about 1% in the visibility amplitude. We also assumed that only closure phase information would be available, so that the simulated phase observations had large random errors. Photon noise calculations imply that with 5 minute integrations the phase noise should always be limited by the calibration errors and atmospheric phase fluctuations, rather than by photon statistics. The visibility amplitude signal to noise should be in excess of 100 if the visibility amplitude is higher than 0.01, so that the amplitudes are also dominated by the effects of calibration errors. To simulate this performance, we included a 2 degree additive random error in the visibility phases and 1% multiplicative (calibration) and 0.1% additive errors to the visibility amplitudes. In addition to this, 360 degree random errors were added to the phase of each siderostat to simulate the effects of the atmosphere. The simulations generated a complex visibility for each wavelength channel every 5 minutes. The simulated data were checked to verify that the visibilities were high enough to phase the array. For a third magnitude star, this requirement implies that the visibility be at least 0.3 in the 900 nm wavelength channel for all of the tracking baselines. We assumed a duty cycle of 75%, with 3 integrations of 5 minutes each followed by a 5 minute gap. Observations extended over three eight hour periods, one for each configuration.

The model source image, shown in Figure 8, is a 1.6 milliarcsecond diameter, star-like object. The image in Figure 8 has been convolved with a gaussian shaped beam of 0.19 milliarcseconds in diameter so that it represents the ideal image which could be produced by BOA. The source structure is

more complicated than we expect to see on most stars, but is certainly in the realm of possibilities. There is a large prominence-like feature containing 10% of the total flux to the upper left and three groups of star spots. In addition, the star is limb darkened: the surface brightness at the limb is only one half the central value. This amount of limb darkening is consistent with that expected for a star of spectral type F-III. For simplicity, we have assumed no color-dependent features for the simulated star. Such variations would have complicated the present simulations, but will routinely be included in actual images from BOA.

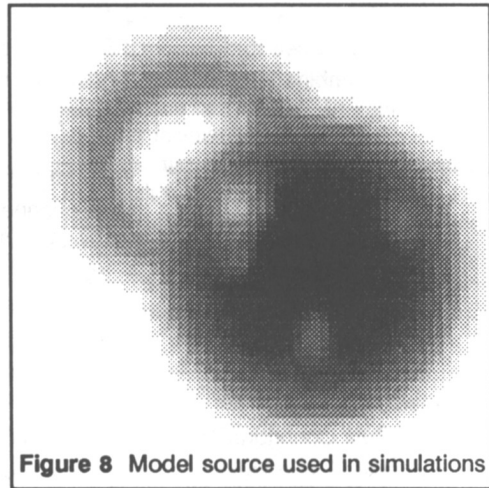


Figure 8 Model source used in simulations

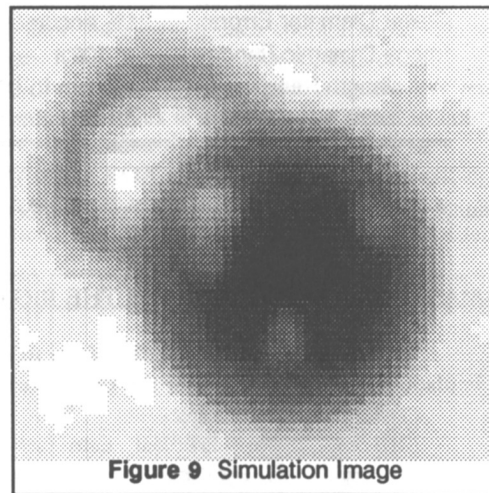


Figure 9 Simulation Image

The final reconstructed image for this simulation is shown in Figure 9. Reconstruction of the image was done using standard self-calibration techniques, and did not take advantage of the fact that phase errors between different wavelength bands will be correlated. All of the features present in the source can be seen in the reconstructed image. Based on these results, we expect that fainter objects will still yield reliable images, and that the overall performance of BOA for imaging will be excellent.

SUMMARY

In conclusion, optical interferometry has great promise for imaging celestial objects with an angular resolution previously achieved only at radio wavelengths using VLBI techniques. Completion of BOA will be an important step in realizing the goal of producing high resolution images at optical wavelengths.

REFERENCES

- M. M. Colavita 1990, in SPIE Proc. 1237 *Amplitude and Intensity Spatial Interferometry*, ed. J. B. Breckinridge, 80.
- D. L. Fried 1965, *J. Opt. Soc. Am.*, **55**, 1427.
- R. Hanbury Brown, J. Davis, and R. Allen 1974, *Mon. Not. Roy. Astr. Soc.* **167**, 121.
- J. A. Hughes and D. J. Hutter 1990, in SPIE Proc. 1237 *Amplitude and Intensity Spatial Interferometry*, ed. J. B. Breckinridge, 10.
- M. G. Lacasse and W. A. Traub 1988, Proc. ESO Conf. No. 29 *High Resolution Imaging by Interferometry*, 959.
- D. Mozurkewich, D. J. Hutter, K. J. Johnston, R. S. Simon, M. Shao, M. M. Colavita, D. H. Staelin, B. E. Hines, J. L. Hershey, J. A. Hughes, and G. H. Kaplan 1988, *Astron. J.*, **95**, 1269.
- D. Mozurkewich, D. J. Hutter, K. J. Johnston, and R. S. Simon 1990, in SPIE Proc. 1237 *Amplitude and Intensity Spatial Interferometry*, ed. J. B. Breckinridge, 120.
- D. Mozurkewich, K. J. Johnston, R. S. Simon, P. P. Bowers, R. A. Gaume, D. H. Hutter, M. M. Colavita, M. Shao, and X. P. Pan 1991, *Astron J.*, submitted.
- M. Shao, M. M. Colavita, B. E. Hines, D. H. Staelin, D. J. Hutter, K. J. Johnston, D. Mozurkewich, R. S. Simon, J. L. Hershey, J. A. Hughes, G. H. Kaplan 1988, *Astron. Astrophys.*, **193**, 357.
- M. Shao, M. M. Colavita, B. E. Hines, J. L. Hershey, J. A. Hughes, G. H. Kaplan, K. J. Johnston, D. Mozurkewich, R. S. Simon, X. P. Pan 1990, *Astron J.* **100**, 1701.
- R. S. Simon, D. Mozurkewich, K. J. Johnston, R. A. Gaume, D. J. Hutter, P. F. Bowers, M. M. Colavita, and M. Shao 1990, in SPIE Proc. 1237 *Amplitude and Intensity Spatial Interferometry*, ed. J. B. Breckinridge, 316.